Electronic Supporting Information

In-Situ Nitrogen-Doped Mesoporous Carbon Nanofibers as Flexible Freestanding Electrodes for High-Performance Supercapacitors

Jian Tan,[a] Yulai Han,[*cd] Liang He,[a] Yixiao Dong,[a] Xu Xu,[a] Dongna Liu,[a] Haowu Yan,[a] Qiang Yu,[a] Congyun Huang,[a] and Liqiang Mai [*ab]

[a.] State Key Laboratory of Advanced Technology for Materials Synthesis and Processing, International School of Materials Science and Engineering, Wuhan University of Technology, Wuhan 430070, P. R. China. *E-mail: mlq518@whut.edu.cn.

[b.] Department of Chemistry, University of California, Berkeley, CA 94702, USA.

[c.] School of New Materials and New Energies, Shenzhen Technology University, Shenzhen 518118, P.R. China. *E-mail: hanyulai@sztu.edu.cn.

[d.] School of Applied Technology, Shenzhen University, Shenzhen 518118, P. R. China.

Experimental Section

Preparation of $Mg(OH)_2$/DMF Precursor Solution

In a typical synthesis, the magnesium hydroxide ($Mg(OH)_2$) nanoplates were synthesized by a simple refluxed method. Generally, 12.8 g $Mg(NO_3)_2 \cdot 6H_2O$ and 4.0 g NaOH were dissolved in 115.2 mL and 36.0 mL deionized (DI) water, respectively. Then, the NaOH solution was dropwisely added to the $Mg(NO_3)_2 \cdot 6H_2O$ solution. Afterward, the mixture solution was transferred into a glass flask and heated to 100 °C in an oil bath and kept refluxing for 3 h under continuous stirring, followed by naturally cooling down to room temperature. The precipitation was then collected by centrifugation and rinsed with DI water for several times, the product was dispersed in N,N-dimethylformamide (DMF) to form $Mg(OH)_2$ solution (3 wt.%). Thus, the precursor solution was obtained.

Electrospinning of PAN/$Mg(OH)_2$ Nanofibers

First, PAN (Mw = 85,000) was slowly added into $Mg(OH)_2$/DMF solution (10 wt.%), after stirred at 70 °C for 2 h, a viscous and homogeneous precursor solution was obtained. Afterward, the precursor solution was transferred into a 10 mL plastic syringe with a stainless steel needle connected to a high-voltage power supply. The grounded electrode was linked to the collector wrapped by aluminum (Al) foil. The relative humidity, temperature, distance between needle tip and collector and flow rate were determined as 40%, 25 °C, 16 cm and 0.05 mm min^{-1}, respectively. Subsequently, the precursor solution was electrospun into fibers. With a fixed voltage of 13 kV applied to the solution during the spinning process in the system (electrospinning equipment: SS-2534H from UCALERY Co., Beijing, China), the jet was stretched by electrostatic force, then a large quantity of uniform composite nanofibers were generated and deposited on the Al drum (at ~30 r min^{-1}). Finally, the PAN/$Mg(OH)_2$ nanofibers network was obtained.

In-situ Synthesis of the Flexible Freestanding N-doped Mesoporous Carbon Nanofibers (N-MCNFs)

Firstly, the as-prepared PAN/$Mg(OH)_2$ nanofibers network was cut into many slices (Fig.S1(b)) after electrospinning. Afterward, these slices were peeled off from the Al foil and pre-oxidized by annealing in air at 280 °C, with a heating rate of 2 °C min^{-1} and held at this temperature for 1 h. The stabilized PAN/$Mg(OH)_2$ nanofibers network was then placed in an alumina boat at the center of tube

furnace and carbonized under nitrogen (99.999%) flow, with the temperature increasing to 900 °C by a rate of 5 °C min^{-1} and reserved at this temperature for 5 h. Subsequently, the sample was etched by 2 M HCl solution, and the MgO was removed effectively. Then, the nanofibers network was washed with DI water and ethanol several times, followed by drying at 60 °C overnight in vacuum. Finally, the flexible freestanding N-MCNFs-900 electrode material was obtained. For comparison, the $Mg(OH)_2$-free PAN nanofibers carbonized at 900 °C are denoted as CNFs-900.

Characterization

The X-ray diffraction patterns of the samples were obtained with a Bruker D8 Advance powder X-ray diffractometer using Cu Kα radiation. Thermal gravimetric analysis (TGA) was conducted on a thermogravimetric analyzer (TGA Q500, Thermal Analysis Instruments, USA) in air or N_2 with a flow rate of 50 mL min^{-1} and a temperature ramp rate of 10 °C min^{-1}. To characterize the morphology of the samples, scanning electron microscope (SEM) images were recorded by a JEOL JSM-7100F field emission SEM (FESEM), transmission electron microscope (TEM) and high resolution TEM images were collected with a JEM-2100F TEM. Raman spectra were measured using a Renishaw INVIA micro-Raman spectroscopy system. X-ray photoelectron spectroscopic analysis was carried out on VG Multilab 2000. The Brunauer-Emmett-Teller (BET) surface areas of the samples were measured using Tristar II 3020 instrument by nitrogen adsorption at 77 K. The elemental composition (C, H, O and N) was recorded by Vario EL cube CHNO elemental analyzer. The evolution of the water contact angle was measured by the contact angle measurement system (D8 ADVANCE X-Ray diffractometer).

Electrochemical measurements

The characterizations of electrochemical performance of the samples were performed by conducting cyclic voltammetry (CV) and galvanostatic charge-discharge (GCD) using a typical three-electrode configuration in 6 M KOH electrolyte at room temperature. In the measurement, the as-synthesized materials were directly employed as the working electrode, the platinum (Pt) sheet was used as counter electrode, and the saturated calomel electrode (SCE) was employed as reference electrode. The working electrode was prepared by pressing the electrode material (with mass loading of ~0.5 mg) and a nickel foam (used as the current collector, specific capacitance = 0 F g^{-1}, corresponding CV curve at a scan rate of 100 mV s^{-1} as shown in Fig. S8) together without any additional binders or conductive additives. All the electrochemical

measurements in 6 M KOH aqueous solution were conducted at room temperature. CV and GCD tests were performed using an electrochemical workstation of CHI 605E (Chenhua Instruments Co. Ltd., Shanghai). Electrochemical impedance spectroscopy (EIS) measurement was performed with an amplitude of 10 mV, from 0.01 to 10^5 Hz. In general, the specific capacitance (C_s) of a single electrode can be calculated in the three-electrode configuration by following equation (1):

$$C_s = I\Delta t/(m\Delta V) \quad (1)$$

where C_s (F g^{-1}) is the specific capacitance, I(A) represents the discharge current, Δt(s) is the discharge time, ΔV(V) corresponds to the voltage range after a full charge or discharge process excluding the IR drop, and m (g) refers to the mass of the electrode materials on the working electrode.

The electrochemical performance of supercapacitors with N-MCNFs-900 and CNFs-900 electrode materials were tested by conducting CV and GCD using a two-electrode cell configuration in 6 M KOH electrolyte at room temperature. The calculations of the capacitances were followed by the equations displayed.

$$C_m = I\Delta t/(m\Delta V) \quad (2)$$

$$E = 0.5\ C_m\ (\Delta V)^2 \quad (3)$$

$$P = 3.6\ E/\Delta t \quad (4)$$

where C_m (F g^{-1}) represents the measured cell capacitance, I (A) is the discharge current, Δt (s) is the discharge time, m (g) is the total mass of the active material on the two electrodes, ΔV (V) refers to the potential window excluding the IR drop during the discharge process, E (W h kg^{-1}) refers to the energy density, P (kW kg^{-1}) corresponds to the power density.

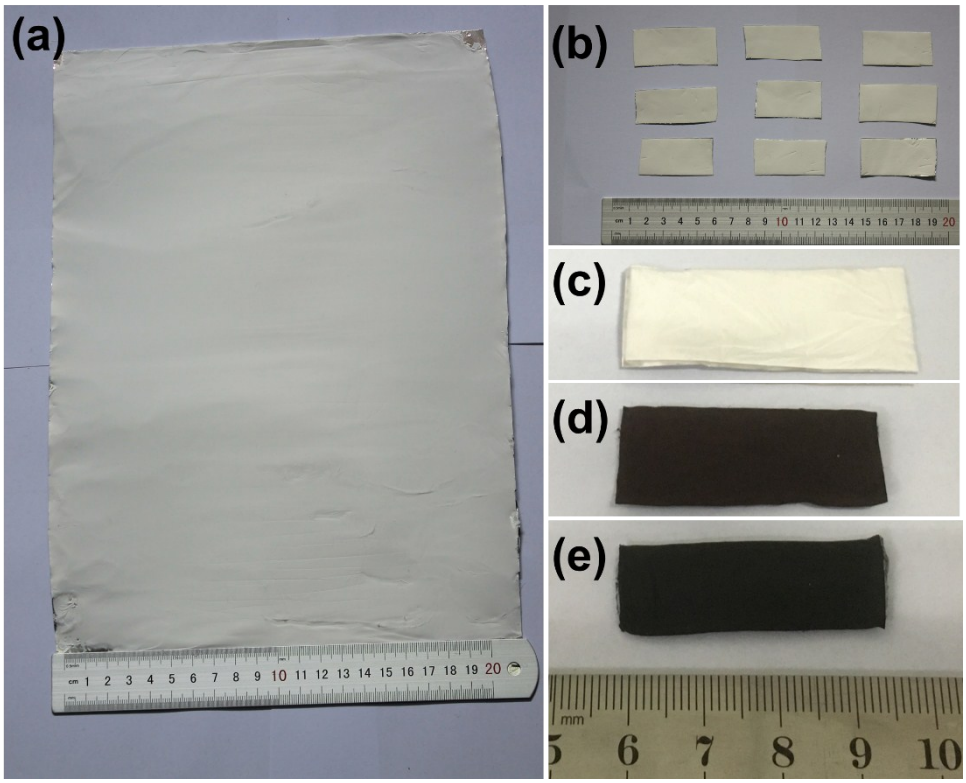

Fig. S1. Photographs of PAN-derived carbon nanofibers network: (a) aluminum foil after electrospinning for 10 h with one ordinary syringe needle, (b) some slices with electrospun nanofiber network, (c) original slice (white color), (d) the slice after pre-oxidation (dark-brown color), and (e) the slice after annealing at 900 °C (black color).

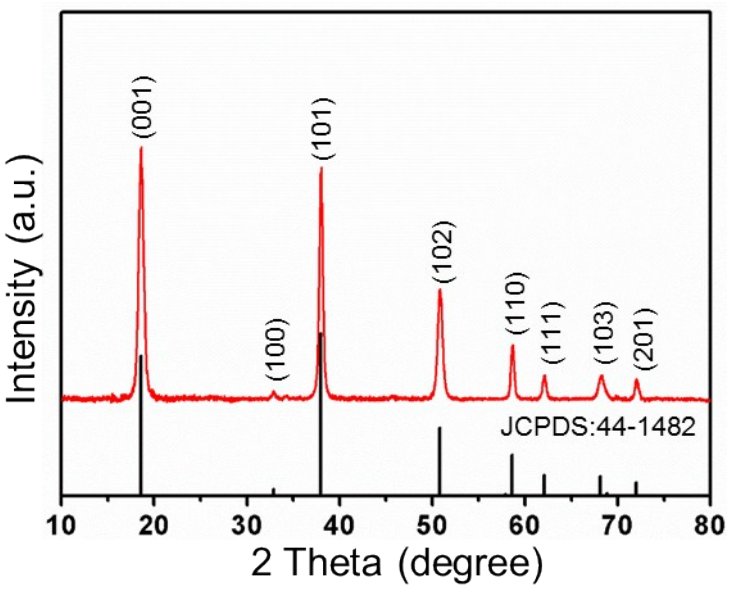

Fig. S2. XRD pattern of the prepared $Mg(OH)_2$ nanoplates.

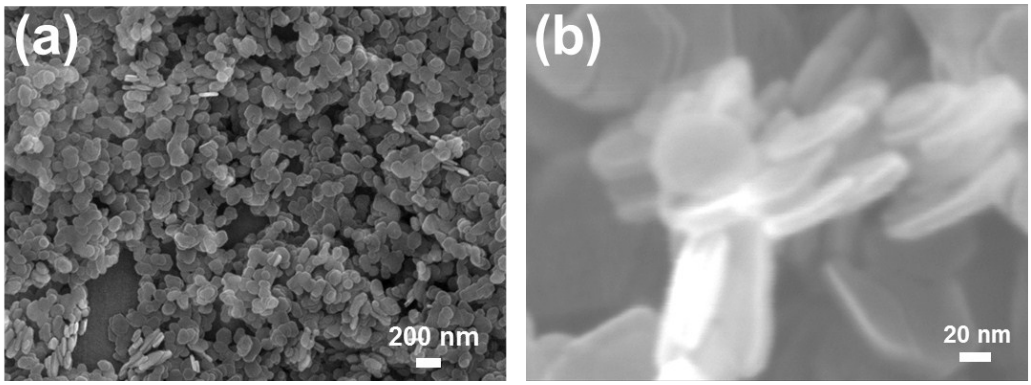

Fig. S3. (a) Low-magnification and (b) high-magnification FESEM images of the $Mg(OH)_2$ nanoplates.

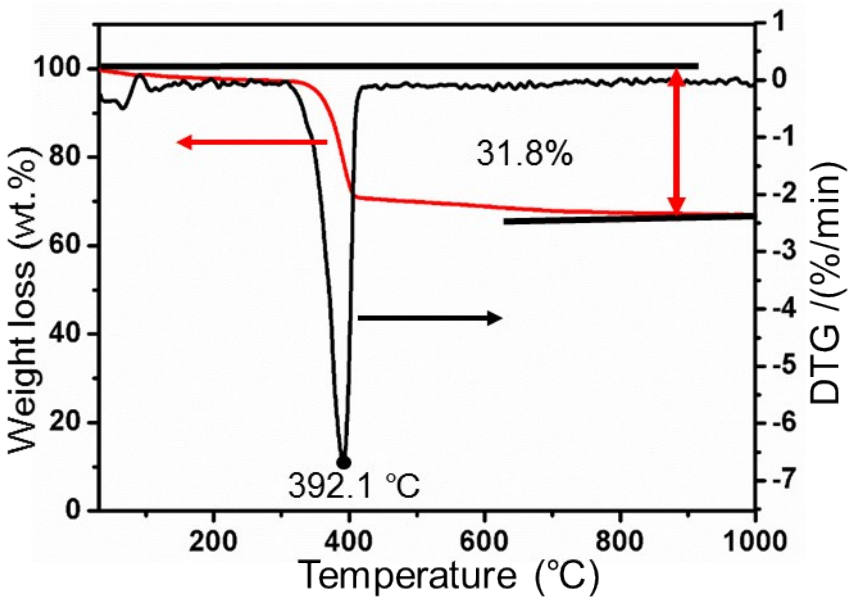

Fig. S4. TGA and DTG curves of the $Mg(OH)_2$ nanoplates.

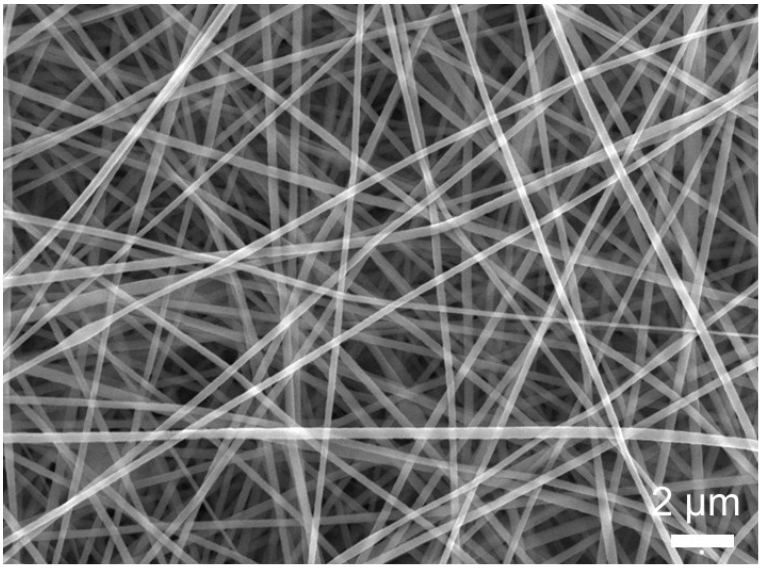

Fig. S5. Low-magnification SEM image of PAN/$Mg(OH)_2$ composite nanofibers.

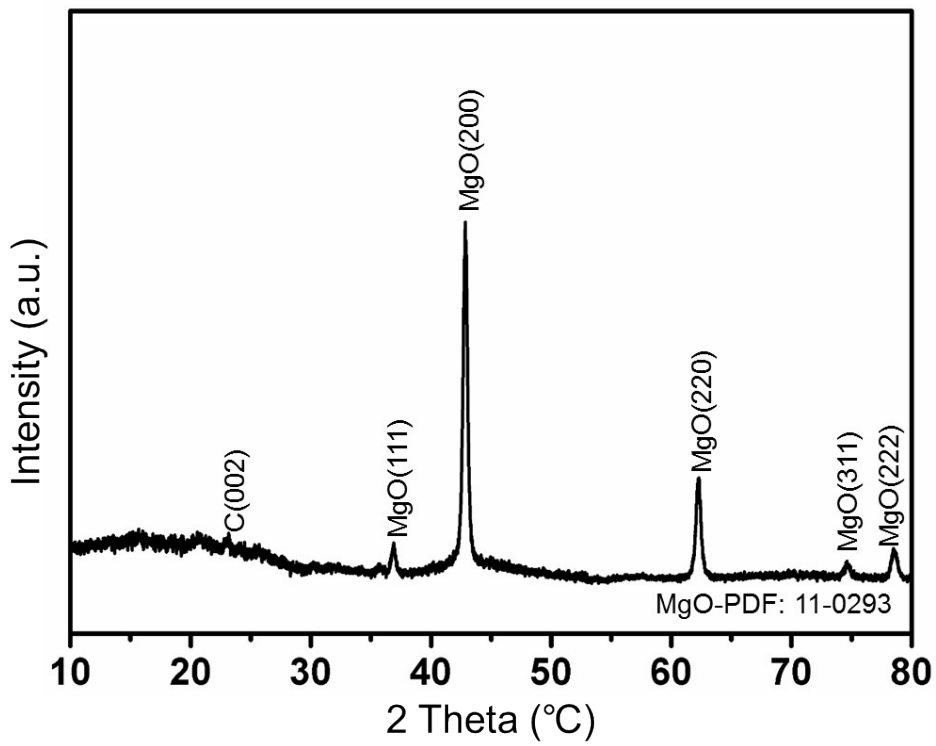

Fig. S6. The wide-angle XRD pattern of the MgO/carbon composite after carbonization at 900 °C.

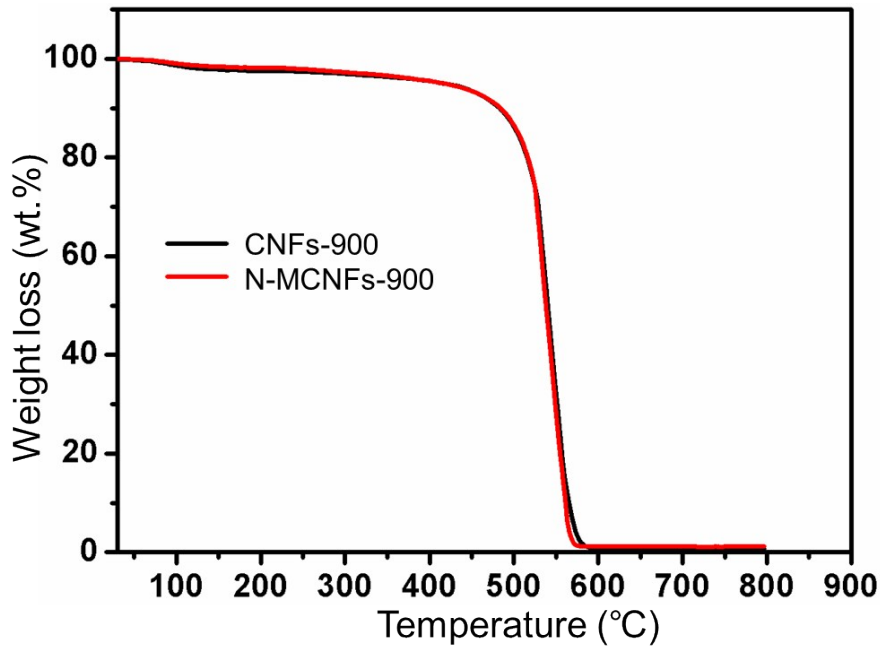

Fig. S7. TGA curves of the CNFs-900 and N-MCNFs-900 under air.

Table S1. Elemental analysis results of the electrode materials.

Sample	C (wt.%)	O (wt.%)	N (wt.%)	H (wt.%)
CNFs-900	76.1	9.3	6.2	0.7
N-MCNFs-900	76.15	11.55	6.5	0.7

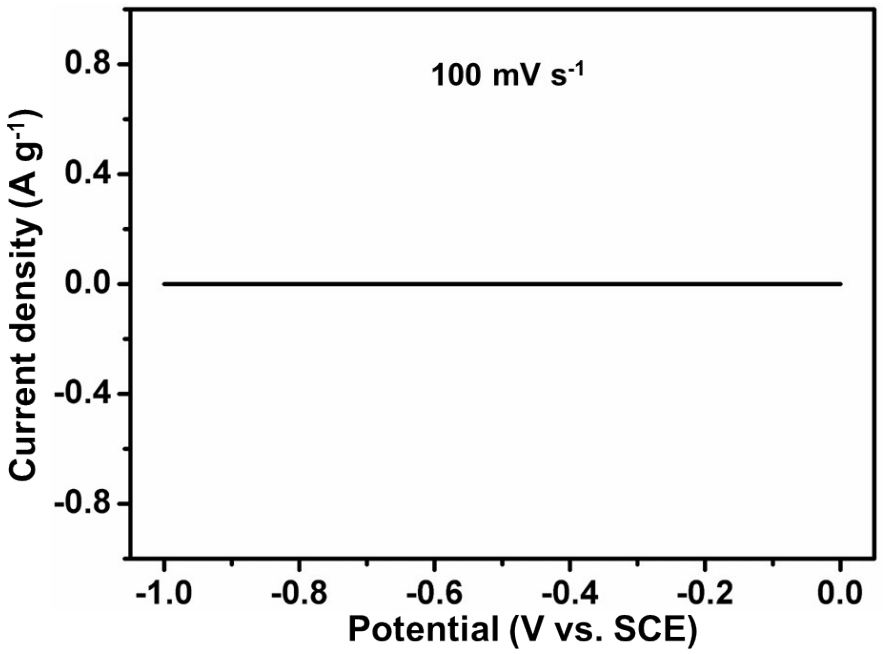

Fig. S8 The CV curve of pure nickel current collectors at 100 mV s^{-1}.

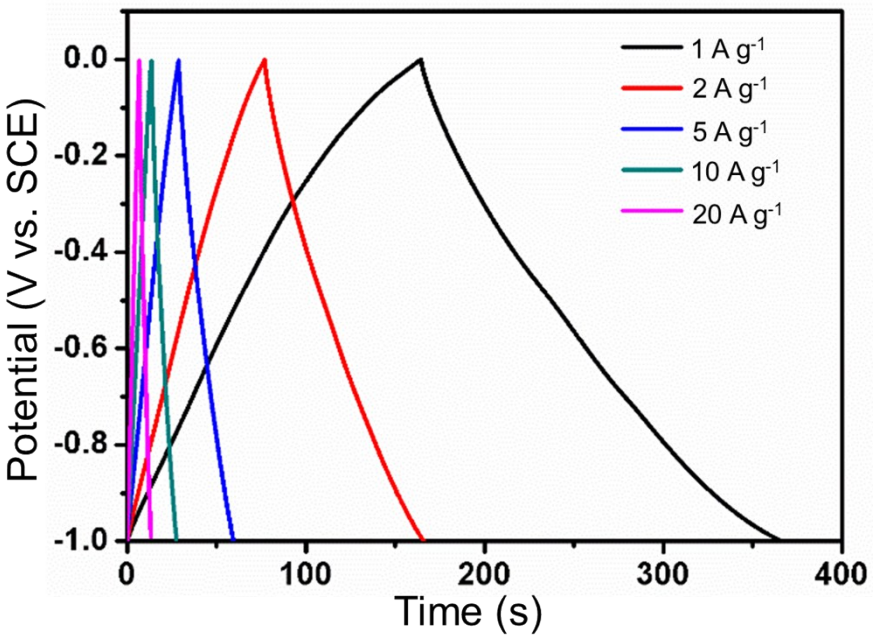

Fig. S9. GCD curves of CNFs-900 at different current densities in three-electrode configuration under 6 M KOH electrolyte.

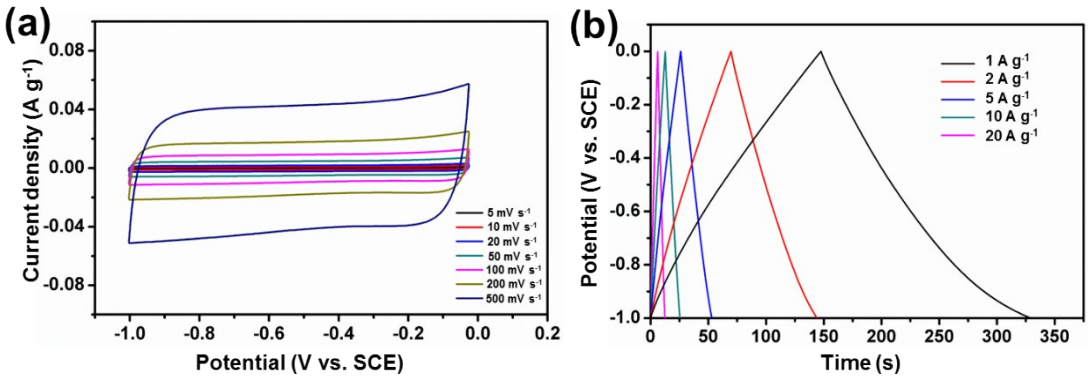

Fig. S10. (a) CV curves of CNFs-900 at different scan rates in two-electrode configuration (b) GCD curves of CNFs-900 at different current densities in two-electrode configuration under 6 M KOH electrolyte

Table S2. Pore parameters of N-MCNFs-900 and CNFs-900.

Sample	BET surface area (m^2 g^{-1})	Pore volume (cm^3 g^{-1})	Average pore diameter (nm)
N-MCNFs-900	926.40	0.42	4.26
CNFs-900	208.03	0.23	7.76

Table S3. Comparison of the specific capacitances (C_s) of some N-doped porous carbon-based electrode materials for supercapacitors in the literature.

Materials	Electrolyte	Current density (A g^{-1})	C_s (F g^{-1})	References
N-MCNFs-900	6 M KOH	1	327.3	This work
H-NMC-2.5	1 M H_2SO_4	0.2	262	1
	6 M KOH	0.2	227	
SWNT/rGO	1 M H_2SO_4	1	305	2
p-BC-N-25	2.0 M H_2SO_4	1	195.44	3
PNCNs	1 M H_2SO_4	0.1	311	4

CA-GA-2	6 M KOH	1	220	5
	1 M H_2SO_4	1	300	
N-CNFs-900	6 M KOH	1	202	6
N-CNTs/CF	6 M KOH	1	206.3	7
NG	6 M KOH	1	282	8
TC	1 M H_2SO_4	0.5	286.6	9
CTNC	1 M H_2SO_4	0.1	166 ± 5	10
	6 M KOH	0.1	124 ± 3	
HPC	1 M H_2SO_4	1	383	11
MCS	5 M H_2SO_4	1	211	12
NHHNC	6 M KOH	1.0	322	13
HPCNFs-N	2.0 M H_2SO_4	1.0	307.2	14
CNCs-800	6 M KOH	1.0	248	15
HNCNCs-800	6 M KOH	1	313	16
OMFLC-N	0.5 M H_2SO_4	1	855	17
	2 M Li_2SO_4	1	780	

Table S4 Comparison of the Energy density and Power density of some N-doped porous carbon-based electrode materials for supercapacitors in the literature.

Materials	Electrolyte	Current density ($A\ g^{-1}$)	Energy density（$W\ h\ kg^{-1}$）	Power density ($kW\ kg^{-1}$)	References
N-MCNFs-900	6 M KOH	1	42.5	10	This work
CNFs-900	6 M KOH	1	25	4.1	
PNCNs	1 M H_2SO_4	0.1	17.7	1.1	4
N-CNFs-900	6 M KOH	0.25	7.11	89.57	6
TC	1 M H_2SO_4	0.5	31.3	11.8	9
HPC	1 M Na_2SO_4	1	60.3	18	11
HPCNFs-N	2 M H_2SO_4	1	10.96	25	14
hCNCs	6 M KOH	1	10.90	22.22	16
OMFLC-N	0.5 M H_2SO_4	1	36.5	42.5	17
	2 M Li_2SO_4	1	54.5	44.0	

References

1 J. Wei, D. Zhou, Z. Sun, Y. Deng, Y. Xia and D. Zhao, Adv. Funct. Mater., 2013, **23**, 2322-2328.

2 D. Yu, K. Goh, H. Wang, L. Wei, W. Jiang, Q. Zhang, L. Dai and Y. Chen, *Nat. Nanotechnol.*, 2014, **9**, 555-562.

3 L. F. Chen, Z. H. Huang, H. W. Liang, W. T. Yao, Z. Y. Yu and S. H. Yu, *Energy Environ. Sci.*, 2013, **6**, 3331-3338.

4 Y. Y. Wang, B. H. Hou, H. Y. Lü, C. L. Lü and X. L. Wu, *ChemistrySelect*, 2016, **1**, 1441-1447.

5 L. Zhao, L. Z. Fan, M. Q. Zhou, H. Guan, S. Y. Qiao, M. Antonietti and M. M. Titirici, *Adv. Mater.*, 2010, **22**, 5202-5206.

6 L. F. Chen, X. D. Zhang, H. W. Liang, M. Kong, Q. F. Guan, P. Chen, Z. Y. Wu and S. H. Yu, *ACS Nano*, 2012, **6**, 7092-7102.

7 S. He, H. Hou and W. Chen, *J. Power Sources*, 2015, **280**, 678-686.

8 H. M. Jeong, J. W. Lee, W. H. Shin, Y. J. Choi, H. J. Shin, J. K. Kang and J. W. Choi, *Nano Lett.*, 2011, **11**, 2472-2477.

9 Y. Q. Zhao, M. Lu, P. Y. Tao, Y. J. Zhang, X. T. Gong, Z. Yang, G. Q. Zhang and H. L. Li, *J. Power Sources*, 2016, **307**, 391-400.

10 M. Zhong, E. K. Kim, J. P. McGann, S.-E. Chun, J. F. Whitacre, M. Jaroniec, K. Matyjaszewski and T. Kowalewski, *J. Am. Chem. Soc.*, 2012, **134**, 14846-14857.

11 P. Yu, Z. Zhang, L. Zheng, F. Teng, L. Hu and X. Fang, *Adv. Energy Mater.*, 2016, **6**, 1601111.

12 W. Li, D. Chen, Z. Li, Y. Shi, Y. Wan, J. Huang, J. Yang, D. Zhao and Z. Jiang, *Electrochem. Commun.*, 2007, **9**, 569-573.

13 J. Liang, C. C. Wang and S. Y. Lu, *J. Mater. Chem. A*, 2015, **3**, 24453-24462.

14 L.-F. Chen, Y. Lu, L. Yu and X. W. Lou, *Energy Environ. Sci*., 2017, DOI: 10.1039/C7EE00488E.

15 Y. Tan, C. Xu, G. Chen, Z. Liu, M. Ma, Q. Xie, N. Zheng and S. Yao, *ACS Appl. Mater. Interfaces*, 2013, **5**, 2241-2248.

16 J. Zhao, H. Lai, Z. Lyu, Y. Jiang, K. Xie, X. Wang, Q. Wu, L. Yang, Z. Jin and Y. Ma, *Adv. Mater.*, 2015, **27**, 3541-3545.

17 T. Lin, I. W. Chen, F. Liu, C. Yang, H. Bi, F. Xu and F. Huang, *Science*, 2015, **350**, 1508-1513.